ELSEVIER

Dynamics of Atmospheres and Oceans 23 (1996) 81–98

dynamics of atmospheres and oceans

Direct and large eddy simulations of stratified homogeneous shear flows

Ulrich Schumann

Deutsche Forschungsanstalt für Luft- und Raumfahrt (DLR), Institut für Physik der Atmosphäre, Oberpfaffenhofen, 82230 Wessling, Germany

Received 7 July 1994; revised 26 January 1995; accepted 9 March 1995

Abstract

An overview is given on direct numerical simulations and on large eddy simulations of homogeneous turbulence under the impact of shear and stable stratification. We describe the methods used and report on the results of various studies. In particular, the vortex structure of turbulent motions is discussed. Moreover, the dynamics of statistical mean quantities are investigated. The mean variances are compared with experimental data. The turbulent diffusivity tensor for passive species in a stratified shear flow is computed. Moreover, a simple model is described which allows us to estimate the vertical diffusivities for heat and momentum for such flows when the vertical velocity variance or the dissipation rate are known.

1. Introduction

Stratified shear flows are important in the stratosphere, in the free stable troposphere, in the stable atmospheric boundary layer (ABL) over cooled surfaces, and in the ocean. See Hopfinger (1987), Fernando (1991) and Etling (1993) for reviews. In this paper, we summarize briefly some recent results for ABL and then concentrate on homogeneous stratified shear flows, with uniform shear and stratification (without mean rotation). In the homogeneous case, all turbulence statistics are independent of the spatial coordinates but vary with time. The paper summarizes the results of various recent numerical simulations, using either direct numerical simulation (DNS) resolving the whole spectrum of motions up to the dissipating scale, or using large-eddy simulation (LES), resolving only the main energy and flux carrying motion structures while the small-scale turbulent transports are approximated by a proper subgrid-scale (SGS) model. We will show that DNS and LES provide insight into the vortex structure of such flows, its basic

SSDI 0377-0265(95)00423-8

dynamics, the vertical transport of heat and momentum, and the anisotropic diffusion of passive species.

Turbulence in stratified shear flows depends strongly on the Richardson number (Richardson, 1920). Let S denote the vertical velocity shear and s the vertical potential temperature gradient

$$S = \frac{\mathrm{d}U}{\mathrm{d}z}, \quad s = \frac{\mathrm{d}\Theta}{\mathrm{d}z} > 0 \tag{1}$$

then the Brunt–Väisälä frequency N and the gradient Richardson number Ri are defined as

$$N = (\beta g s)^{1/2}, \quad \mathrm{Ri} = \frac{N^2}{S^2} \tag{2}$$

Here, β is the thermal volumetric expansion coefficient, and g is the acceleration of gravity. As summarized by Farrell and Ioannou (1993), for $\mathrm{Ri} < 0.25$ somewhere in the flow, small perturbances in inviscid fluid may grow exponentially. In general one expects that existing turbulence decays with time when $\mathrm{Ri} > 0.25$. In viscous flows this limit may be smaller. But even for $\mathrm{Ri} = O(1)$, transient growth of perturbations can be substantial, and may cause overturning for $\mathrm{Ri} < 0.4$. Turbulent motions get enhanced by shear at small Richardson numbers. Hence, turbulent mixing may occur under non-stationary conditions at all Richardson numbers.

The flow state depends also on the timescale of turbulence, e.g. $\tau = l/q$, where l denotes the integral lengthscale and $q = (2E)^{1/2}$ the velocity scale as a function of the kinetic energy of turbulent motions E. (Alternative timescales may be defined in terms of the dissipation rate ε of kinetic energy.) Dimensionless numbers that relate the internal timescale to the outer timescales S^{-1} and N^{-1}, are the shear number Sh and the inverse Froude number Fi

$$\mathrm{Sh} = S\tau, \quad \mathrm{Fi} = \mathrm{Fr}^{-1} = N\tau, \quad \mathrm{Ri} = \frac{\mathrm{Fi}^2}{\mathrm{Sh}^2} \tag{3}$$

The shear number determines the importance of mean shear relative to turbulent shear. In strongly stratified flows, the inverse of the Froude number Fr becomes important. For Fi greater than a critical value of about 3, turbulent mixing dies out (collapse of turbulence) (see Hopfinger, 1987; Etling, 1993).

Turbulence in homogeneous shear flows has been measured by Rohr et al. (1988) in salt-stratified water. Reliable data for homogeneous air flows are available only for neutral stratification (Tavoularis and Karnik, 1989). The early measurements by Webster (1964) were obtained from a wind-tunnel experiment at rather a low Reynolds number with notable departure from a quasi-steady state.

Homogeneous stratified shear flows have been investigated by DNS in Gerz et al. (1989), Gerz and Schumann (1989, 1991) and Holt et al. (1992). They investi-

gated the flow dynamics as a function of Richardson numbers in between zero and 1.32. On current computers, such simulations can be performed on grids with typically 128^3 grid points. For such grids, DNS is restricted to a Prandtl number of order unity and to a turbulent Reynolds number, based on root-mean square velocity fluctuations and Taylor's microscale, of less than about 50. For atmospheric flows, much larger Reynolds numbers are of interest. For this reason, the DNS method has been extended into a LES method by Kaltenbach et al. (1994). This extends formally the Reynolds number to infinity. However, the range of resolved scales is still limited by numerical resolution.

With respect to turbulence in the ABL, most previous studies concentrated on the convective and the neutral cases (Schumann, 1993). For comparison of various LES codes to these cases see Nieuwstadt et al. (1993) and Andrén et al. (1994). The stable ABL is much more demanding because of smaller turbulence scales and the tendency to turbulence collapse. Mason and Derbyshire (1990) showed that LES of the stable ABL is possible, giving results broadly similar to observations, and supporting the local scaling arguments of Nieuwstadt (1984). Coleman et al. (1992) found similar results in DNS of a stable ABL at moderate Reynolds number. Mason and Thomson (1992) raised the important issue of stochastic backscatter. They showed theoretically that the subgrid parametrization should be stochastic, and that this substantially improved LES performance in the neutral surface layer. Recently, Brown et al. (1994) extended that work applying LES with stochastic backscatter to the stable ABL. The forcing causes more turbulence and a deeper ABL and better agreement of the velocity profile gradients with observations. For strong stratification, when the turbulence scales with the local fluxes, the turbulence statistics of the ABL become directly comparable to results from homogeneous flows. Other LES models without backscatter may provide similar results (see Sullivan et al., 1994).

Since DNS and LES compute the details of the three-dimensional motions, at least on the energetic scales, they can be used to study the vortex structure and the related transports, as is explained in Section 3.1., based on the work of Rogers and Moin (1987), Gerz (1991), Gerz et al. (1994) and others. For related discussions of other stratified shear flows, see, for example, Lesieur (1993) and Staquet (1993).

Turbulent transport in stably stratified shear flow is strongly anisotropic owing to forcing of downstream turbulent motion by shear and conversion of kinetic energy of vertical motions into potential energy by buoyancy forces (Richardson, 1920). As a consequence, passive species within the flow are mixed by the turbulent motions much more in the horizontal direction than in the vertical. The relation between fluxes and gradients is described by the turbulent diffusivity tensor which is anisotropic and asymmetric in general. The diffusion tensor has been measured for neutral homogeneous shear flows in a wind tunnel by Tavoularis and Corrsin (1985) and computed using DNS by Rogers et al. (1989). For stratified turbulence, the diffusion tensor has been evaluated from DNS and LES (Kaltenbach et al., 1991, 1994), as summerized in this overview.

With respect to practical diffusion problems in stratified shear flows, the vertical diffusivity component is the most important one. For diffusion from a line

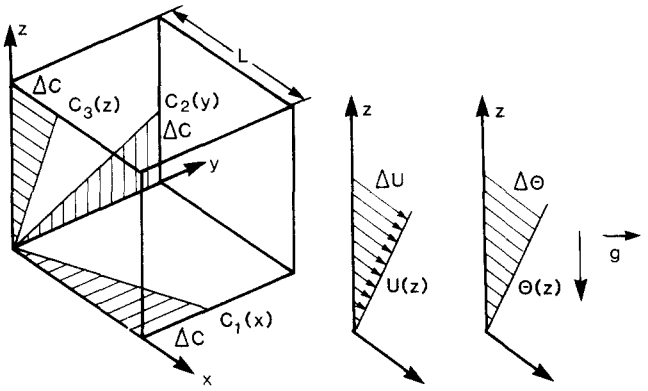

Fig. 1. Computational domain and mean profiles (from Kaltenbach et al., 1994. Reprinted by permission of Cambridge University Press).

source, a Gaussian plume model (assuming a constant but anisotropic diffusivity tensor D_{ij} results in second-order moments of the concentration field

$$\sigma_{11} = 2t\left(D_{33}S^2t^2/3 + D_{13}St + D_{11}\right), \quad \sigma_{13} = \sigma_{31} = 2D_{13}t + D_{33}St^2,$$
$$\sigma_{33} = 2tD_{33} \tag{4}$$

as functions of time t (Konopka, 1995). This shows clearly the importance of the vertical diffusivity D_{33} dominating horizontal dispersion when $D_{33}t^2S^2 > 3D_{11}$ (see also Monin and Yaglom, 1971).

Simple relationships are required to estimate the magnitude of the mixing properties. Such relationships have been deduced, mainly for strongly stratified atmospheric and oceanic flows, on the basis of the energy budgets using simple closure assumptions for stationary flows (see, e.g. Itsweire et al., 1993). The present paper summarizes a simple model which takes into account the deviation from stationarity and applies to both stratified and unstratified shear flows.

2. The numerical method used for DNS and LES

The numerical method has been described in detail by Gerz et al. (1989) and Kaltenbach et al. (1994). It simulates the turbulent flow in a cubic domain (see Fig. 1), with side-lengths L. The mean velocity $(U, 0, 0)$ and the mean temperature Θ have uniform gradients in the vertical coordinate z while being constant in the two other directions. All mean gradients are kept fixed in time. The turbulent fluctuations relative to these mean values are $u_i = (u,v,w)$ for velocity, and θ for temperature.

Shear imposes a problem with respect to the boundary conditions. The common choice of boundary conditions in DNS of homogeneous turbulence is periodicity in all space directions. However, in the presence of shear a field which is initially periodic in the vertical direction soon becomes non-periodic. Thus the common

periodicity condition cannot be used in that direction. Rogers and Moin (1987) and Holt et al. (1992) applied a method using time-dependent coordinate transformation which corresponds to a Lagrangian reference frame, so that the flow may be assumed to be periodic in the direction of the transformed coordinate. This makes it possible to apply Fourier-spectral approximations of the fields with respect to this coordinate. The disadvantage of this approach is the need for remeshing at a frequency $(1/2)\mathrm{d}U/\mathrm{d}z$, which causes interpolation errors of the aliasing type. We use the alternative approach, where the equations are discretized in the Eulerian reference frame using the so-called shear-periodic boundary condition (Schumann, 1985). This condition assumes periodicity in a direction which varies as a function of time. It corresponds to continuous remapping by applying horizontal periodicity and avoids interruptions at discrete times. This type of boundary condition is not applicable to Fourier spectral approximations in the vertical but can easily be implemented in a finite difference scheme. Both approaches produce very similar results (Holt et al., 1992).

The motion fields follow the continuity equation for an incompressible fluid with constant density ρ, the equations of motion including buoyancy resulting from density fluctuations and gravity g in the Boussinesq approximation, and the conservation laws for heat and mass as a function of spatial coordinates $x_i = (x,y,z)$ and time t. The density fluctuation is a linear function of temperature with a constant volumetrical expansion coefficient β.

In the study of Kaltenbach et al. (1994), the SGS turbulent transport is modelled using turbulent diffusivities, the so-called Smagorinsky model

$$\nu_t = (c_{\mathrm{SGS}}\Delta)^2(2S_{ij}S_{ji})^{1/2}, \quad \gamma_t = \frac{\nu_t}{\mathrm{Pr}_{\mathrm{SGS}}} \tag{5}$$

for velocity and temperature, respectively. Here, $S_{ij} = \partial u_i/\partial x_j + \partial u_j/\partial x_i$ is the resolved velocity deformation tensor, $c_{\mathrm{SGS}} = 0.17$ is the Smagorinsky coefficient, and $\mathrm{Pr}_{\mathrm{SGS}}$ is the turbulent Prandtl number of SGS motions. The velocity deformation tensor is evaluated excluding the mean shear $\mathrm{d}U/\mathrm{d}z$ in order to avoid unrealistically strong damping for decaying turbulence. In fact, this model is justified theoretically only for locally isotropic turbulence where the local deformation induced by turbulence is large compared with the mean shear. In this sense, the mean shear should be negligible. The value of the Smagorinsky coefficient is based on the inertial subrange theory as described in Schmidt and Schumann (1989). The same theory gives $\mathrm{Pr}_{\mathrm{SGS}} \cong 0.42$, but larger values are expected for stable stratification (Schumann, 1991; Canuto and Minotti, 1993). Also, backscatter causes a larger value (about 0.6–0.7 for neutral stratification) (see Mason and Thomson, 1992).

It should be noted that simulations with 128^3 grid points do not yet resolve the inertial subrange. As a consequence of deviations from local isotropy, the SGS shear number $\mathrm{Sh}_{\mathrm{SGS}} = Sl/u'$ is of order unity. In the inertial subrange, the shear number scales with $\Delta x^{4/3}$. Hence, a reduction of $\mathrm{Sh}_{\mathrm{SGS}}$ by a factor of 10 would be desirable, but this requires about 5.6 times more grid points or 1000 times more computer power.

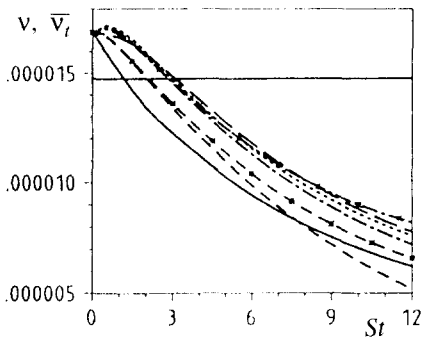

Fig. 2. Non-dimensional mean turbulent viscosity ν_t (in units of SL^2, with shear S and scale L of the box forming the computational domain) of LES for various models and molecular viscosity ν of DNS versus shear time St. The various lines refer to various models as explained in Gerz and Palma (1994). In particular, the continuous horizontal line corresponds to a case with constant viscosity ν, the continuous curve describes the standard Smagorinsky model, and the other curves denote results from a model with a transport equation of subgrid-scale energy of various complexity (from Gerz and Palmer, 1994. Reprinted by permission of Kluwer Academic Publishers.).

Kaltenbach et al. (1994) compared DNS and LES results using this Smagorinsky model. They found that LES and DNS give the same results for weak stratification, when the constant molecular viscosity of the DNS is set equal to the initial mean turbulent viscosity of the LES. Hence, a LES is nothing more than a DNS with spatially and temporally variable viscosity. In the present cases, the spatial variability of the SGS viscosity is small, as also found by Métais and Lesieur (1992) for unsheared homogeneous turbulence. However, LES energy spectra decay more slowly than DNS spectra at high wavenumbers. Moreover, in LES the viscosity adjusts to the decaying turbulence at large scales (see Fig. 2). Therefore, LES gives a better approximation than a DNS at a given resolution for studies of high Reynolds number flows and allows for a wider range of Richardson numbers.

Gerz and Palma (1994) tested variants of two SGS models, one based on the first-order model using a budget for the SGS kinetic energy (as in Schumann, 1991) and the other based on Smagorinsky's closure. Tests with grid sizes of 64^3 showed that the details of the SGS closure are not critical and become even less important when resolution is increased. Production and dissipation of SGS energy are the two largest terms in the energy budget. The Smagorinsky model simply assumes that they are equal. For $\mathrm{Ri} = 0.5$, the time tendency of the SGS energy is rather large, and this explains some differences in the effective viscosity (see Fig. 2). We have also tested the code with a new stochastic backscatter model (Schumann, 1995). For isotropic turbulence, the effect of such forcing is small.

3. Examples

3.1. Vortex structure and microfronts

Structures in turbulence are often viewed as regions of strong coherent vorticity (Lesieur, 1993) and zones of concentrated field gradients, sometimes called mi-

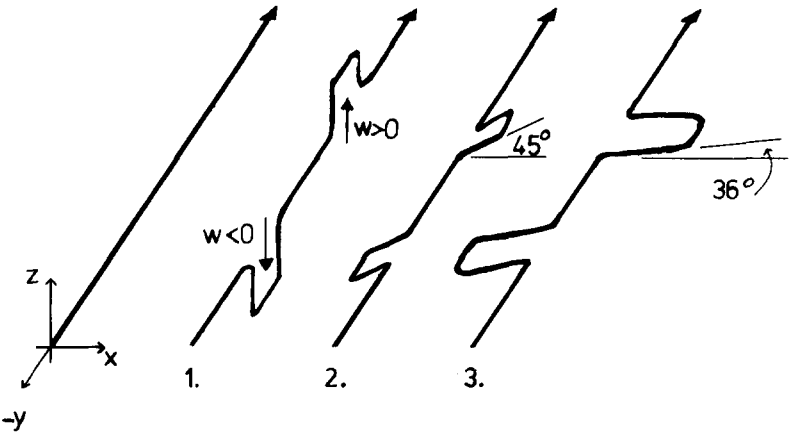

Fig. 3. Schematic illustration of the creation of horseshoe eddies (from Gerz et al., 1994. Reprinted by permission of the American Institute of Physics.).

crofronts (Gerz et al., 1994). In shear flows without inflection points (in contrast to shear layers), horseshoe and hairpin structures of fluctuating vorticity have been found in unstratified boundary layers but also for homogeneous shear flows both in neutrally (Rogers and Moin, 1987) and weakly stably stratified situations (Gerz, 1991). Horseshoe-shaped vortex structures are present in flows with low to moderate Reynolds numbers, whereas hairpin-shaped vortices typically occur in high-Reynolds-number flows with large shear numbers.

As sketched in Fig. 3, horseshoe vortices form and decay transiently in four steps:

(1) an initial disturbance resulting from vertical motions forms vertically distorted vortices;

(2) the vertically deflected vortex curves get rotated by the mean rotating flow;

(3) stretching of the structure is strongest owing to the mean strain when they pass 45°;

(4) further rotation by the mean rotation reduces the inclination angle until the vortices are dissipated.

Gerz (1991) found that the strongest vorticity is distributed around $\vartheta = 25°$ in a stratified shear flow with $\mathrm{Ri} = 0.13$, but that most of the coherent horseshoe vortices are found at angles of approximately 36°; as in unstratified shear flows (Rogers and Moin, 1987) (see Fig. 4).

In wall-bounded shear layers the mean velocity profile is curved. This causes a preference of horseshoe vortices with 'head-up' orientation such that the curved part (the head) of the horseshoe forms in the outer region of the boundary layer whereas the legs of the horseshoe stay closer to the wall. In contrast, head-up and head-down horseshoes form at equal frequency in homogeneous turbulence with constant shear.

The flow in between the horseshoe legs is very efficient in transporting fluid and related momentum, heat, and other fluid properties. In between the legs, head-up horseshoe vortices pump fluid upwards, while head-down vortices pump fluid

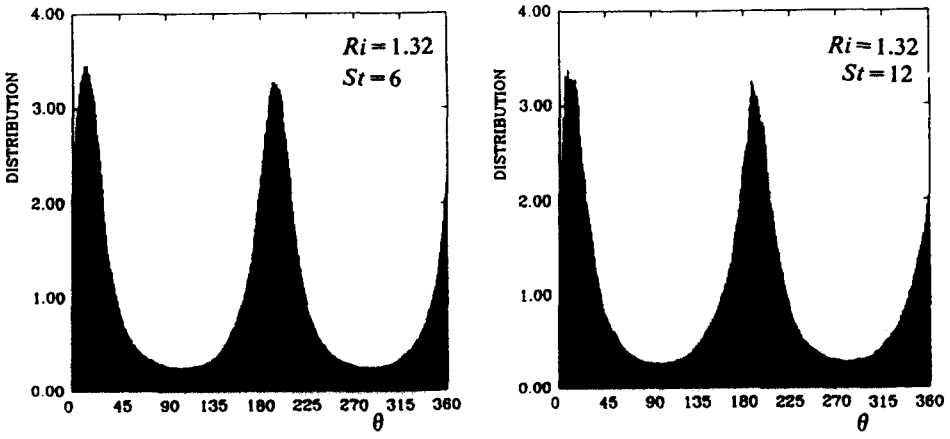

Fig. 4. Frequency of inclination angle of vortex vectors relative to downstream coordinate. (a) Ri = 0.13, (b) Ri = 1.32 (from Gerz, 1991. Reprinted by permission of Kluwer Academic Publishers.).

downwards. As shown by Gerz et al. (1994) (see Fig. 5), this causes the formation of microfronts with strong gradients of the transported fields in the direction normal to the horseshoes. In a thermally stratified fluid, at moderate Richardson numbers, head-up vortices transport cold fluid upwards and hence, cause cold microfronts, whereas head-down vortices transport warm fluid downwards causing cold microfronts.

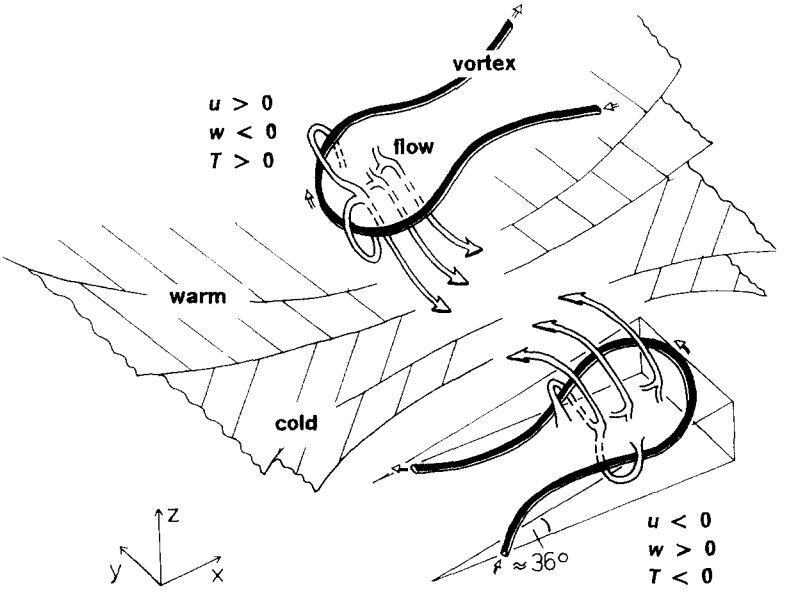

Fig. 5. Sketch of two horseshoe vortices forming a pair (from Gerz et al., 1994. Reprinted by permission of the American Institute of Physics.).

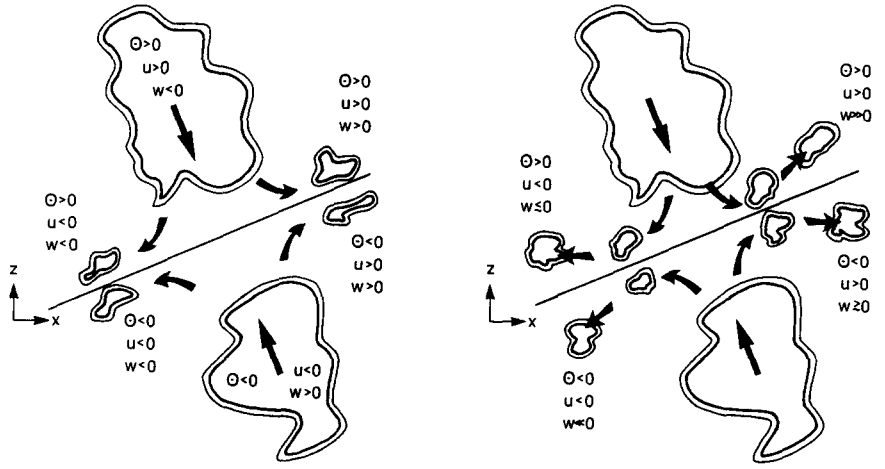

Fig. 6. Illustration of the collision of fluid lumps and the resultant transport of momentum and heat by smaller scale collision products in neutral (left) and stratified (right) shear flows (from Gerz and Schumann, 1995. Reprinted by permission of Springer-Verlag GmbH & Co. KG.).

The microfronts represent also regions of strong shear with spanwise vorticity. When the Reynolds number is high enough these vortex layers become dissipated slowly and may reach stronger vorticity than the horseshoe vortices. Such layers of maximum vorticity magnitude have been observed by Gerz et al. (1994). The layers are relatively thin vertically and have largest extent in the inclined downstream direction.

Collision of fluid lumps in between adjacent head-up and head-down horseshoe vortices causes smaller scale fragments which may cause counter-gradient momentum transfer (see Fig. 6). In moderately stably stratified flows, this collision of fluid lumps of different buoyancy also causes counter-gradient heat transfer at small scales (Gerz, 1993; Gerz and Schumann, 1995). This provides a mechanistic explanation of this phenomenon which supplements energetic considerations as in Schumann (1987).

At very strong stratification, horseshoe vortices do not form. Instead, Gerz (1991) found horizontally large but vertically thin sheets of maximum vorticity (see Fig. 7), which are inclined at rather small angles (see Fig. 4). Such sheets of vorticity are also found, with $\vartheta = 0°$, in simulations of strongly stratified unsheared turbulence (Métais and Herring, 1989). Staquet (1993) shows that the vortex parts of such flows interact strongly with wavy motion parts.

3.2. Dynamics and diffusion in homogeneous stratified shear turbulence

LES of homogeneous turbulence for neutrally and stably stratified shear flow at gradient-Richardson numbers Ri in between zero and one have been performed by Kaltenbach et al. (1994). They investigated the dynamics and transport properties

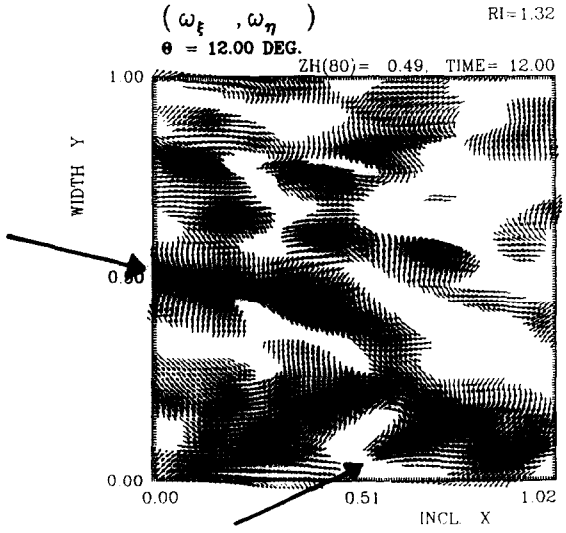

Fig. 7. Vortex structure at strong stratification as indicated by vorticity vectors in a plane inclined by $\vartheta = 12°$ relative to the horizontal. Ri = 1.32 (from Gerz, 1991. Reprinted by permission of Kluwer Academic Publishers.).

of such flows. For $\mathrm{Ri} \leqslant 0.5$, the computed normalized variances and covariances are within the range of data of a large set of measurements in laboratory and atmospheric flows (see, e.g. Fig. 12). Also the growth rate, the shear number, and the shape of spectra agree generally well with corresponding experimental observations. For neutral stratification, the turbulence grows about exponentially with time (see Fig. 8(a)), approaching a constant shear number of about $Sw'^2/\varepsilon \cong 2$, and a growth rate $G_0 = P/\varepsilon = 1.54 \pm 0.05$. The state of turbulence changes very slowly near a stationary Richardson number of about 0.13. For $\mathrm{Ri} \geqslant 0.25$, both the

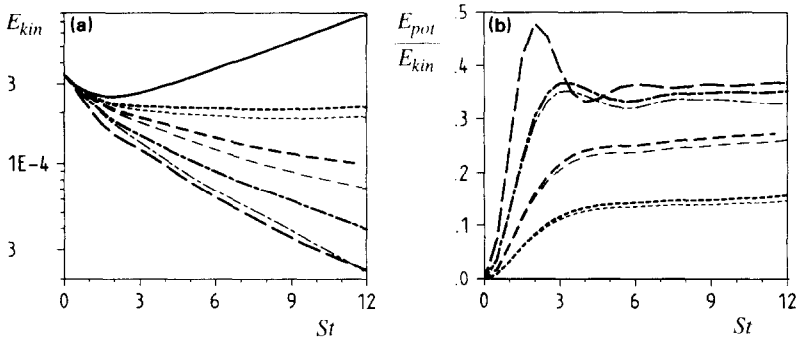

Fig. 8. (a) Kinetic energy versus time in shear units for various Richardson numbers Ri; continuous line, 0, short dashed line 0.13, medium dashed line, 0.25, dashed dotted line, 0.5, long dashed line, 1.0. (b) Ratio of potential to kinetic energy versus shear time, for the same Ri-values (from Kaltenbach et al., 1994. Reprinted by permission of Cambridge University Press.).

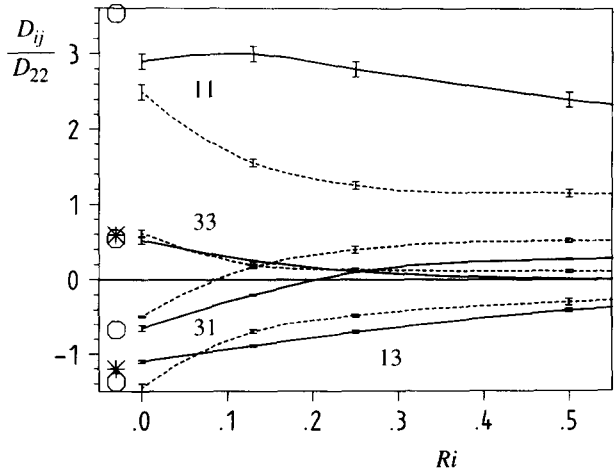

Fig. 9. Diffusivity tensor versus Ri. Continuous line with error bars from LES results. For Ri = 0, results from Rogers et al. (1990) are included, but they are plotted at positions for slightly negative Ri values to separate them from the LES results. Stars represent data from Tavoularis and Corrsin (1985). Dashed curves are from the SOC model. At Ri = 0, the curve pairs, from top to bottom, belong to D_{ij} with $ij = 11$, 33, 31, 13 (from Kaltenbach et al., 1994. Reprinted by permission of Cambridge University Press.).

kinetic and the potential energy decay with time. For $0.25 \leqslant \mathrm{Ri} \leqslant 0.5$, the turbulent flow state becomes self-similar in the sense of approaching constant normalized flow statistics, as for example in Fig. 8(b), after a shear time of about 6 when the initial value of the inverse Froude number is small. For Fi greater than a critical value of about 3 turbulent mixing dies out as observed in experiments (see, e.g. Ivey and Imberger, 1991). In this case the final statistics depend on the history of mixing in the fully turbulent regime.

For analysis of the turbulent transport of passive species, the simulations treat three passive species with uniform gradients of mean concentrations C in either vertical, downstream or cross-stream direction (see Fig. 1). From the results, the full diffusivity tensor has been evaluated by relating the computed turbulent fluxes of concentration fluctuations c with the given mean gradients

$$\overline{u_i c} = -D_{ij}\frac{\partial C}{\partial x_j} \tag{6}$$

Mean values of D_{ij}/D_{22} for different Ri, as obtained by the LES, are presented in Fig. 9. This figure also contains the results obtained by Rogers et al. (1989) from DNS for neutral shear flow and measurements of Tavoularis and Corrsin (1985). The dashed curves represent the results from a second-order closure (SOC) model. For neutral flow, D_{11} is about three times larger than D_{33}, and D_{33} is roughly half the value of D_{22}. This is a consequence of anisotropic velocity fluctuations and shear. Both off-diagonal components are negative and $D_{13} < D_{31} < 0$, as can be explained by SOC models. For increasing stratification, the vertical diffusivity D_{33} becomes much smaller than the horizontal ones because of buoyancy suppressing

vertical motions. The differences between downstream and cross-stream diffusivities become smaller. The asymmetry of the tensor components depends strongly on Ri. D_{31} changes sign at $\mathrm{Ri} \cong 0.2$ because buoyancy contributes more strongly than gradient fluxes to the production of vertical fluxes of a tracer with downstream mean gradient. The SOC model accounts for the given anisotropic Reynolds stresses and roughly describes the same trends but gives much less anisotropy at strong stratification, presumably because of neglect of anisotropic length and time-scales as defined by Tavoularis and Corrsin (1985).

3.3. A model for vertical diffusivities of heat and momentum

In order to estimate vertical diffusivities as a function of Richardson number, for given dissipation rate ε or for given vertical velocity variance $w'^2 = \overline{w^2}$, Schumann (1994) and Schumann and Gerz (1995) deduced a simple model. As a consequence of the budget of kinetic energy the vertical diffusivities for momentum K_m and heat $K_\mathrm{h} \cong D_{33}$ are related to shear $S = \mathrm{d}U/\mathrm{d}z$, the Brunt–Väisälä frequency N and the dissipation rate ε by

$$K_\mathrm{m} = c_\mathrm{m} \frac{\varepsilon}{\overline{S^2}}, \quad c_\mathrm{m} = \frac{G}{1 - \mathrm{Ri}_f G} \tag{7}$$

$$K_\mathrm{h} = c_\mathrm{h} \frac{\varepsilon}{\overline{N^2}}, \quad c_\mathrm{h} = \frac{\mathrm{Ri}_f G}{1 - \mathrm{Ri}_f G} \tag{8}$$

The coefficient c_h is often quoted as the 'mixing efficiency' (see Itsweire et al., 1993). Here, $G = P/(\varepsilon + B)$ is a measure for the growth rate of kinetic energy due to shear production $P = -\overline{uw}S$, dissipation ε and buoyancy destruction $B = \beta g \overline{w\theta}$; $G > 1$ for flows in which shear production dominates as in neutral shear flows, $G = 1$ for stationary turbulence near a 'stationary Richardson' number $\mathrm{Ri} = \mathrm{Ri}_\mathrm{s}$, and $G < 1$ for decaying turbulence at strong stratification. The flux Richardson number $\mathrm{Ri}_\mathrm{f} = \mathrm{Ri}/\mathrm{Pr}_\mathrm{t} = B/P$ enters as a function of Ri and the turbulent Prandtl number $\mathrm{Pr}_\mathrm{t} = K_\mathrm{m}/K_\mathrm{h}$. For closure, the model assumes a linear relationship between dissipation, shear and vertical velocity variance

$$\varepsilon = A_\mathrm{S} w'^2 S \tag{9}$$

with A_S as an empirical model coefficient (equal to the inverse shear number). This model looks similar to classical dissipation closure models when written as $\varepsilon = A_\mathrm{S} w'^3 / l_w$, but fixes the mixing length as $l_w = w'/S$. This appears to be natural for strongly sheared flows. Hunt et al. (1988) suggested that such a model gives a good approximation also for stratified flows, and our results (see Fig. 10), support this relation for $0 \leqslant \mathrm{Ri} < 1$.

The turbulent Prandtl number (see Fig. 11(a)) and the growth rate of kinetic energy (Fig. 11(b)) are specified by means of some interpolation functions of Richardson number

$$\mathrm{Pr}_\mathrm{t} = \mathrm{Pr}_{\mathrm{t}0} \exp[-\mathrm{Ri}/(\mathrm{Pr}_{\mathrm{t}0}\mathrm{Ri}_{\mathrm{f}\infty})] + \mathrm{Ri}/\mathrm{Ri}_{\mathrm{f}\infty} \tag{10}$$

$$G = G_0^{(1 - \mathrm{Ri}/\mathrm{Ri}_\mathrm{s})} \tag{11}$$

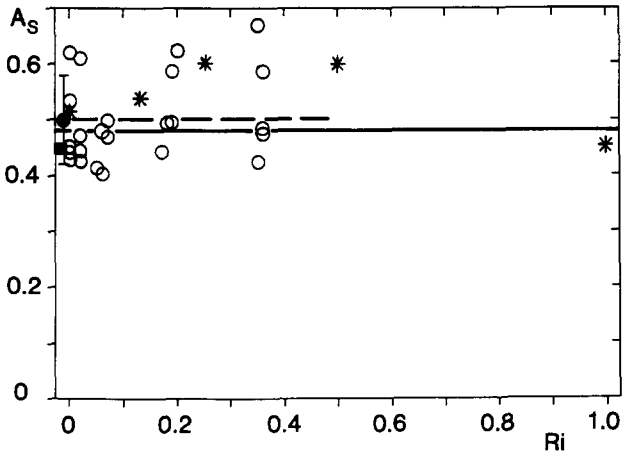

Fig. 10. Dissipation scaled by shear and vertical velocity variance, $A_S = \varepsilon/(w'^2 S)$, versus gradient Richardson number Ri. Data from Rohr (1985) from salt-water (circles), from Tavoularis and Karnik (1989) from a wind tunnel (filled circle with error bar), and the LES results (stars). The square indicates the boundary layer estimate of Hunt et al. (1988) (from Schumann and Gerz, 1995. Reprinted by permission of the American Meteorological Society.).

Model coefficients are determined from the LES results of Kaltenbach et al. (1994) and laboratory measurements of Tavoularis and Karnik (1989) for neutral stratification in a wind tunnel, and from Rohr et al. (1988) for stratified shear

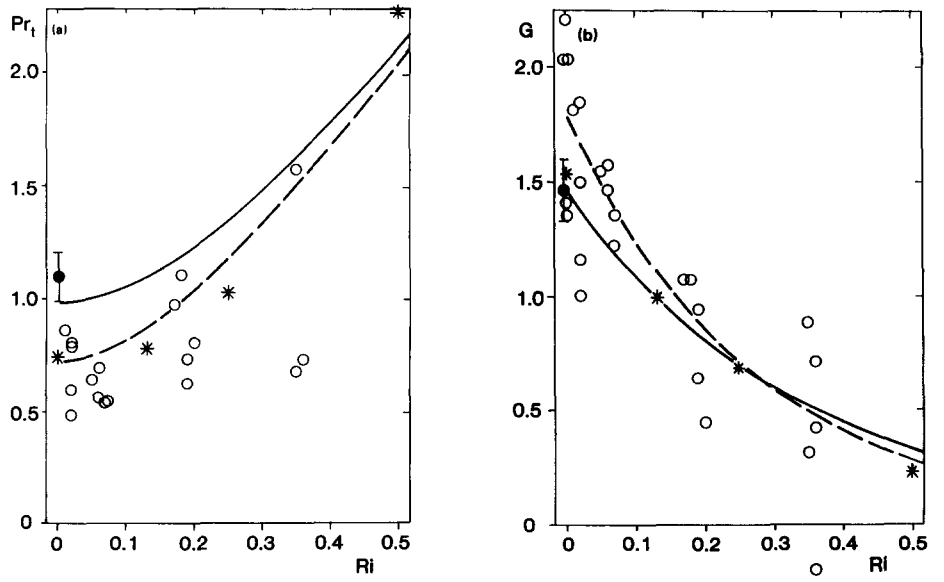

Fig. 11. (a) Turbulent Prandtl number $Pr_t = K_m/K_h$ versus Ri. Symbols as in Fig. 10. The continuous curve depicts the interpolation for air, the dashed curve for salt-water. (b) Growth factor $G = P/(B+\varepsilon)$ versus Ri (from Schumann and Gerz, 1995. Reprinted by permission of the American Meteorological Society.).

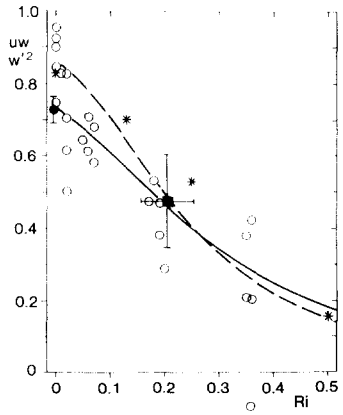

Fig. 12. Stress coefficient $\alpha_{uw} = -\overline{uw}/w'^2$ versus Ri. Symbols as in Fig. 10. Filled square with error bars: Nieuwstadt (1984) (from Schumann and Gerz, 1995. Reprinted by permission of the American Meteorological Society.).

turbulence in a salt-water tank (data tabulated in Schumann, 1994). The coefficient values are $A_S = 0.5$, $\mathrm{Pr}_{t0} = 0.98$, $\mathrm{Ri}_{f\infty} = 0.25$, $G_0 = 1.47$, $\mathrm{Ri}_s = 0.13$, for air, and slightly different values for salt-water (see Schumann and Gerz, 1995).

When comparing mixing properties in the atmosphere and in the ocean, one has to note the rather large molecular Schmidt number of salt diffusing in water (about 500) while the corresponding molecular Prandtl number of thermal diffusion in air is about 0.7. At high Reynolds numbers, one generally expects that the large-scale turbulent motions become independent of the Prandtl number, at least for neutral stratification. However, for strong stratification, the vertical diffusivity is limited by small-scale mixing once the available kinetic energy is consumed to provide the potential energy required for vertical displacements. Such small-scale processes will depend on molecular diffusion. The results for the model compare well with data from laboratory experiments in air or salt-water, with measurements in the ABL and in the stable troposphere, and with results from the numerical simulations (see, e.g. Fig. 12). It should be stressed that this model applies only for approximately homogeneous turbulent flows at high Reynolds numbers under conditions of equilibrium between kinetic and potential energy, i.e. in the absence of strong gravity wave oscillations. Further analysis (Schumann and Gerz, 1995) shows that the present model also describes the breakdown of mixing for $\mathrm{Fi} > 3$, as in Ivey and Imberger (1991).

4. Conclusions and outlook

We have described various results obtained by DNS or LES of homogeneous turbulence in incompressible stably stratified shear flows. It has been shown that the simulations give insight into the vortex structure of such flows, allow us to compute mean statistics of flows and their temporal dynamics, and give quantita-

tive information on the diffusivity tensor and the vertical transport of heat and momentum.

We found that the LES and DNS give very similar results for weak stratification when the constant molecular viscosity of the DNS is set equal to the mean turbulent viscosity of the LES. At strong stratification, the LES resolves a wider range of energetic scales and gives thus a better approximation to high-Reynolds-number turbulence than a DNS with the same grid numbers. The more energetic motions in the medium wavenumber range cause the inverse Froude number to grow less quickly so that mixing persists longer. Hence, the LES results depend less on flow history than the DNS results. Finally, the LES adjusts its SGS diffusivities to the growing or decreasing level of grid-scale turbulence energy. This makes the LES method superior to the DNS for studies of high-Reynolds-number flows and for a wider range of Richardson and Froude numbers.

However, grids with about 128^3 grid points are much too coarse to resolve the inertial subrange of turbulence. Therefore, the results for small-scale properties depend on the details of the SGS model. For the future, within about a decade from now, one may expect that simulations will become possible with an order of 1000 grid points in each coordinate direction. In view of the current level of development of computers, such simulations require algorithms suitable for parallel computers. Such grids would make it possible to resolve scales truly within the inertial subrange for which the SGS models become much more reliable.

With respect to atmospheric turbulence in the free troposphere and above, it is probably very important to account for the large-scale anisotropy of such flows with much larger horizontal than vertical scales. An important topic here is the formation of turbulent spots owing to locally overturning waves in an otherwise strongly stably stratified fluid. Such overturning waves often result from upward travelling gravity waves with certain horizontal phase speeds that interact with the mean flow at critical levels where the mean flow speed equals the phase speed of the waves. Simulation of such flows requires us to prescribe a suitable gravity wave forcing at the bottom boundary and a non-reflective boundary condition at the top of the domain.

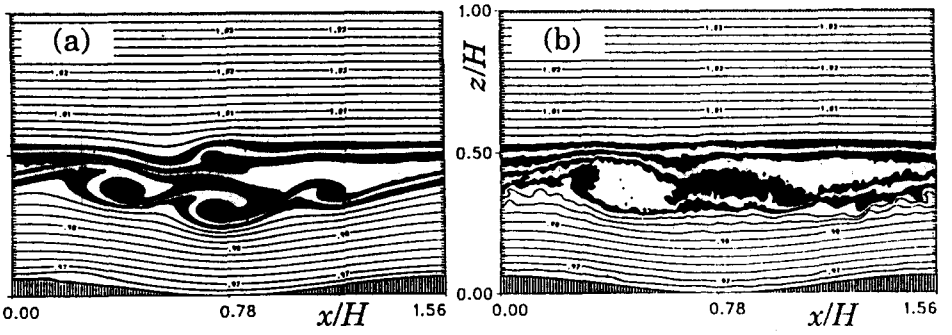

Fig. 13. DNS (a) and LES (b) of a breaking gravity wave at a critical layer (from Dörnbrack and Schumann, 1994. Reprinted by permission of Kluwer Academic Publishers.).

An example of such a flow is given in Fig. 13. It shows the flow field in a stably stratified fluid layer with uniform shear (zero mean flow) where gravity waves of zero phase speed are induced by a lower undulated surface. We clearly observe the turbulence layer caused by breaking gravity waves at and below the critical level (Dörnbrack and Schumann, 1994; Dörnbrack et al., 1995). However, details of this study are beyond the present overview.

Acknowledgements

I thank T. Gerz, A. Dörnbrack, H.-J. Kaltenbach, and J.M.L.M. Palma for the fruitful cooperation from which the results shown in this paper resulted.

References

Andrén, A., Brown, A., Graf, J., Mason, P., Moeng, C.-H., Nieuwstadt, F.T.M. and Schumann, U., 1994. Large-eddy simulation of a neutrally stratified boundary layer: A comparison of four computer codes. Q. J. R. Meteorol. Soc., 120: 1457–1484.

Brown, A.R., Derbyshire, S.H. and Mason, P.J., 1994. Large-eddy simulation of stable atmospheric boundary layers with a revised stochastic subgrid model. Q. J. R. Meteorol. Soc., 120: 1485–1512.

Canuto, V.M. and Minotti, F., 1993. Stratified turbulence in the atmosphere and oceans: a new subgrid model. J. Atmos. Sci., 50: 1925–1935.

Coleman, G.N., Ferziger, J.H. and Spalart, P.R., 1992. Direct simulation of the stably stratified turbulent Ekman layer. J. Fluid Mech., 244: 677–712 (see Corrigendum).

Dörnbrack, A. and Schumann, U., 1994. Numerical simulation of breaking gravity waves below a critical level. In: P.R. Voke, L. Kleiser and J.-P. Chollet (Editors), Direct and Large-Eddy Simulation. Kluwer, Dordrecht, pp. 189–199.

Dörnbrack, A., Gerz, T. and Schumann, U., 1995. Turbulent breaking of overturning gravity waves below a critical level. Appl. Sci. Res., 54: 163–176.

Etling, D., 1993. Turbulence collapse in stably stratified flows: Application to the atmosphere. In: S.D. Mobbs and J.C. King (Editors), Waves and Turbulence in Stably Stratified Flows. Clarendon, Oxford, pp. 1–21.

Farrell, B.F. and Ioannou, P.J., 1993. Transient development of perturbations in stratified shear flow. J. Atmos. Sci., 50: 2201–2214.

Fernando, H.J.S., 1991. Turbulent mixing in stratified fluids. Annu. Rev. Fluid Mech., 23: 455–493.

Gerz, T., 1991. Coherent structures in stratified turbulent shear flows deduced from direct simulations. In: O. Métais and M. Lesieur (Editors), Turbulence and Coherent Structures. Kluwer, Dordrecht, pp. 449–468.

Gerz, T., 1993. Vortex structures and persistent counter-gradient fluxes. In: EUROMECH 305, Dynamics and Geometry of Vortical Structures, Cortona, 28 June–2 July 1993, Abstract. pp. 13–14.

Gerz, T. and Palma, J.M.L.M., 1994. Sheared and stably stratified homogeneous turbulence: Comparison of DNS and LES. In: P.R. Voke, L. Kleiser and J.-P. Chollet (Editors), Direct and Large-Eddy Simulation. Kluwer, Dordrecht, pp. 154–156.

Gerz, T. and Schumann, U., 1989. Influence of initial conditions on the development of stratified homogeneous turbulent shear flow. In: E.H. Hirschel (Editor), Finite Approximations in Fluid Mechanics II, Notes on Numerical Fluid Dynamics Vol. 25. Vieweg, Braunschweig, pp. 142–156.

Gerz, T. and Schumann, U., 1991. Direct simulation of homogeneous turbulence and gravity waves in sheared and unsheared stratified flows. In: F. Durst, B.E. Launder, W.C. Reynolds, F.W. Schmidt and J.H. Whitelaw (Editors), Turbulent Shear Flow Vol. 7. Springer, Berlin, pp. 27–45.

Gerz, T. and Schumann, U., 1995. A note on persistent counter-gradient fluxes in homogeneous turbulence. Theor. Comput. Fluid Dyn., in press.

Gerz, T., Schumann, U. and Elghobashi, S.E., 1989. Direct numerical simulation of stratified homogeneous turbulent shear flows. J. Fluid Mech., 200: 563–594.

Gerz, T., Howell, J. and Mahrt, L., 1994. Vortex structures and microfronts. Phys. Fluids, 6: 1242–1251.

Holt, S.E., Koseff, J.R. and Ferziger, J.H., 1992. A numerical study of the evolution and structure of homogeneous stably stratified sheared turbulence. J. Fluid Mech., 237: 499–539.

Hopfinger, E.J., 1987. Turbulence in stratified fluids: A review. J. Geophys. Res., 92: 5287–5303.

Hunt, J.C.R., Kaimal, J.C. and Gaynor, J.E., 1985. Some observations of turbulence structure in stable layers. Q. J. R. Meteorol. Soc., 111: 793–815.

Hunt, J.C.R., Stretch, D.D. and Britter, R.E., 1988. Length scales in stably stratified turbulent flows and their use in turbulence models. In: J.S. Puttock (Editor), Stably Stratified Flows and Dense Gas Dispersion. Clarendon, Oxford, pp. 285–321.

Itsweire, E.C., Koseff, J.R., Briggs, D.A. and Ferziger, J.H., 1993. Turbulence in stratified shear flows: Implications for interpreting shear-induced mixing in the ocean. J. Phys. Ocean., 23: 1508–1522.

Ivey, G.N. and Imberger, J., 1991. On the nature of turbulence in a stratified fluid. Part I: The energetics of mixing. J. Phys. Ocean., 21: 650–658.

Kaltenbach, H.-J., Gerz, T. and Schumann, U., 1991. Transport of passive scalars in neutrally and stably stratified homogeneous turbulent shear flows. In: A. Johansson and H. Alfredsson (Editors), Advances in Turbulence Vol. 3. Springer, Berlin, pp. 327–334.

Kaltenbach, H.-J., Gerz, T. and Schumann, U., 1994. Large-eddy simulation of homogeneous turbulence and diffusion in stably stratified shear flow. J. Fluid Mech., 280: 1–40.

Konopka, P., 1995. Analytical Gaussian solutions for anisotropic diffusion in a linear shear flow. J. Nonequilibr. Thermodyn., 20: 78–91.

Lesieur, M., 1993. Understanding coherent vortices through computational fluid dynamics. Theor. Comput. Fluid Dyn., 5: 177–193.

Lilly, D.K.., Waco, D.E. and Adelfang, S.I., 1974. Stratospheric mixing estimated from high-altitude turbulence measurements. J. Appl. Meteorol., 13: 488–493.

Mason, P.J. and Derbyshire, S.H., 1990. Large-eddy simulation of the stably-stratified atmospheric boundary layer. Boundary-Layer Meteorol., 53: 117–162.

Mason, P.J. and Thomson, D.J., 1992. Stochastic backscatter in large-eddy simulations of boundary layers. J. Fluid Mech., 242: 51–78.

Métais, O. and Herring, J.R., 1989. Numerical simulation of freely evolving turbulence in stably stratified turbulence. J. Fluid Mech., 202: 117–148.

Métais, O. and Lesieur, M., 1992. Spectral large-eddy simulation of isotropic and stably stratified turbulence. J. Fluid Mech., 239: 157–194.

Miles, J.W., 1961. On the stability of heterogeneous shear flows. J. Fluid Mech., 10: 496–508.

Monin, A.S. and Yaglom, A.M., 1971. Statistical Fluid Mechanics: Mechanics of Turbulence. MIT, Cambridge, MA, p. 638.

Nieuwstadt, F.T.M., 1984. The turbulent structure of the stable, nocturnal boundary layer. J. Atmos. Sci., 41: 2202–2216.

Nieuwstadt, F.T.M., Mason, P.J., Moeng, C.-H. and Schumann, U., 1993. Large-eddy simulation of the convective boundary layer: A comparison of four computer codes. In: F. Durst, R. Friedrich, B.E. Launder, F.W. Schmidt, U. Schumann and J.H. Whitelaw (Editors), Turbulent Shear Flows Vol. 8. Springer, Berlin, pp. 343–367.

Richardson, L.F., 1920. The supply of energy from and to the atmospheric eddies. Proc. R. Soc. London, Ser. A, 97: 354–373.

Rogers, M.M. and Moin, P., 1987. The structure of the vorticity field in homogeneous turbulent flows. J. Fluid Mech., 176: 36–66.

Rogers, M.M., Mansour, N.N. and Reynolds, W.C., 1989. An algebraic model for the turbulent flux of a passive scalar. J. Fluid Mech., 203: 77–101.

Rohr, J.J., Itsweire, E.C., Helland, K.N. and van Atta, C.W., 1988. Growth and decay of turbulence in a stably stratified shear flow. J. Fluid Mech., 195: 77–111.

Schmidt, H. and Schumann, U., 1989. Coherent structure of the convective boundary layer derived from large-eddy simulations. J. Fluid Mech., 200: 511–562.

Schumann, U., 1985. Algorithms for direct numerical simulation of shear-periodic turbulence. In: Lecture Notes in Physics Vol. 218. Springer, Berlin, pp. 492–496.

Schumann, U., 1987. The countergradient heat flux in stratified turbulent flows. Nucl. Eng. Des., 100: 255–262.

Schumann, U., 1991. Subgrid length-scales for large-eddy simulation of stratified turbulence. Theor. Comput. Fluid Dyn., 2: 279–290.

Schumann, U., 1993. Large-eddy simulation of turbulent convection over flat and wavy terrain. In: B. Galperin and S.A. Orszag (Editors), Large Eddy Simulation of Complex Engineering and Geophysical Flows. Cambridge University, Cambridge, pp. 399–421.

Schumann, U., 1994. Correlations in homogeneous stratified shear turbulence. Acta Mech. (Suppl.), 4: 105–111.

Schumann, U., 1995. Stochastic backscatter of turbulence energy and scalar variance from random subgrid-scale fluxes. In: Osborne Reynolds Centenary Symp. 24 May 1994, UMIST, Manchester. Proc. R. Soc. London, Vol. 451.

Schumann, U. and Gerz, T., 1995. Turbulent mixing in stably stratified shear flows. J. Appl. Meteorol., 34: 33–48.

Staquet, C., 1993. Wave/vortex decompositions in stably stratified flows. Theor. Comput. Fluid Dyn., 5: 195–213.

Stillinger, D.C., Helland, K.N. and van Atta, C.W., 1983. Experiments on the transition of homogeneous turbulence to internal waves in a stratified fluid. J. Fluid Mech., 131: 91–122.

Sullivan, P.P., McWilliams, J.C. and Moeng, C.-H., 1994. A subgrid-scale model for large-eddy simulation of planetary boundary-layer flows. Boundary-Layer Meteorol., 71: 247–276.

Tavoularis, S. and Corrsin, S., 1985. Effects of shear on the turbulent diffusivity tensor. Int. J. Heat Mass Transfer, 28: 256–276.

Tavoularis, S. and Karnik, U., 1989. Further experiments on the evolution of turbulent stresses and scales in uniformly sheared turbulence. J. Fluid Mech., 204: 457–478.

Webster, C.A.G., 1964. An experimental study of turbulence in a density-stratified shear flow. J. Fluid Mech., 19: 221–245.